3D PSEUDOLINEAR KALMAN FILTER WITH OWN-SHIP PATH OPTIMIZATION FOR AOA TARGET TRACKING

Sheng Xu[⋆a], *Kutluyıl Doğançay*[⋆◇a] *and Hatem Hmam*[b]

[⋆]Institute for Telecommunications Research, [◇]School of Engineering
[a]University of South Australia, Australia
[b]Cyber and Electronic Warfare Division, DST Group, Australia

ABSTRACT

This paper investigates the problem of how to optimize the path of a single moving own-ship for angle-of-arrival (AOA) target tracking in three-dimensional (3D) space. First, a novel 3D pseudolinear Kalman filter (PLKF) is proposed to reduce computational complexity and to improve stability of an extended Kalman filter solution. This filter consists of an xy-PLKF and a z-PLKF, transforming the nonlinear azimuth and elevation angle measurements into pseudolinear models. We show that when the own-ship and target are at the same height, the z-PLKF will be unbiased. Next, a gradient-descent path optimization algorithm is developed for the xy-PLKF aiming at minimizing the trace of the covariance matrix. Then, a grid search path optimization method is designed for the z-PLKF. Simulation examples verify the effectiveness of the proposed path optimization algorithm.

Index Terms— Three-dimensional, angle-of-arrival, pseudolinear Kalman filter, unbiased condition, path optimization.

1. INTRODUCTION

In 3D angle-of-arrival (AOA) target tracking, the objective is to estimate the target dynamics from azimuth and elevation angle measurements collected by a moving own-ship or spatially-distributed sensors [1, 2]. The own-ship can be an aircraft, vehicle, submarine or any other mobile platform equipped with angle sensors. 3D-AOA tracking has been widely used in both military and civilian areas such as missile tracking and vehicle monitoring. In the AOA tracking problem, the moving path of the own-ship plays a vital role in determining target estimation performance [2, 3]. This paper focuses on the own-ship path optimization based on a 3D pseudolinear estimator to track a moving target.

To estimate the target dynamics in the 3D space, many estimators have been developed before. A 3D one-step pseudolinear estimator (PLE) with bias compensation strategy was proposed in [4]. As the bias compensation cannot make the estimator unbiased, a 3D improved weighted instrumental variable estimator was also developed based on [5]. In [6], another 3D AOA PLE, drawing on [7], was introduced consisting of an xy-PLE and a z-PLE with bias reduction and selective angle measurement strategies. However, as these are batch estimates, their computational complexity will increase as more measurements are collected. To avoid large computational complexity and to be able to track maneuvering targets, in [8, 9, 10], a 2D pseudolinear Kalman filter (PLKF) was developed with better stability than the extended Kalman filter (EKF) [1]. In this paper, we will extend the 2D PLKF into the 3D space using the ideas of 3D-PLE developed in [6].

Many different sensor path optimization strategies have been presented for the AOA target tracking problem. In [11], a gradient-descent path optimization method was proposed aiming to minimize the mean-squared-error (MSE) in the 2D plane. By maximizing the determinant of the Fisher information matrix (FIM), a 2D optimal sensor trajectory of a single mobile sensor was introduced in [12]. In [2], the 2D gradient-descent method was improved by solving a nonlinear programming problem over a set of discrete UAV waypoints to comply with geometric constraints. A grid search method was also introduced to overcome the inaccuracies of the gradient method. For static target localization, different optimal sensor deployment strategies based on optimizing the FIM in 2D and 3D were developed in [13], [14] and [15]. However, these methods cannot be applied directly to moving target tracking.

In this paper, we focus on path optimization for a single moving own-ship tasked with target tracking in the 3D space. The nonlinear noisy angle measurements are transformed into pseudolinear models. First, a 3D PLKF comprised of an xy-PLKF and a z-PLKF is designed. Next, we find that when the own-ship and target are at the same height the z-PLKF will be unbiased. Then, a gradient-descent path optimization algorithm is proposed for the xy-PLKF to minimize its mean squared error (MSE). The optimal z-axis coordinate for the ownship is determined by a grid search optimization algorithm applied to the z-PLKF. The rest of the paper is organized as follows. Section 2 is the problem formulation. The detailed 3D-PLKF algorithm and the unbiasedness condition for the z-PLKF are introduced in Section 3. The path optimization strategies based on the xy-PLKF and z-PLKF are presented in Section 4. The effectiveness of the proposed method is illustrated with simulation examples in Section 5. Finally, the conclusion is drawn in Section 6.

2. PROBLEM FORMULATION

We consider a single moving own-ship equipped with AOA sensors tracking a moving target in 3D space. The AOA sensor acquires 3D angle measurements including an azimuth angle θ_k and an elevation angle ϕ_k (See Fig. 1). The own-ship location is represented by $\boldsymbol{r}_k = [r_{xk}, r_{yk}, r_{zk}]^T$ with velocities $[\dot{r}_{xk}, \dot{r}_{yk}, \dot{r}_{zk}]^T$ at time k. $\boldsymbol{p}_k = [p_{xk}, p_{yk}, p_{zk}]^T$ denotes the target location and $[\dot{p}_{xk}, \dot{p}_{yk}, \dot{p}_{zk}]$ are the target velocities.

The ideal (noiseless) angle measurements can be written as:

$$\theta_k = \tan^{-1}\frac{p_{yk} - r_{yk}}{p_{xk} - r_{xk}}, \quad -\pi < \theta_k \leq \pi \tag{1a}$$

$$\phi_k = \tan^{-1}\frac{p_{zk} - r_{zk}}{||[p_{xk}, p_{yk}] - [r_{xk}, r_{ky}]||}, \quad -\frac{\pi}{2} < \phi_k \leq \frac{\pi}{2} \tag{1b}$$

where $||\cdot||$ means the Euclidean norm and $\tan^{-1}$ is the 4-quadrant

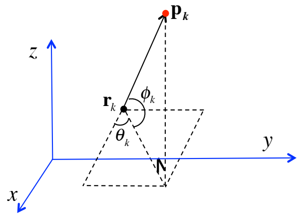

Fig. 1. Azimuth and elevation measurements in 3D.

arctangent. The noisy measurements are

$$\boldsymbol{z}_k = [\theta_k, \phi_k]^T + [n_k, m_k]^T \tag{2}$$

where n_k and m_k are the additive zero-mean independent Gaussian noise with the variances σ_θ^2 and σ_ϕ^2, respectively. In this paper, we assume the noise variances are constants and ignore the effects of clutter and/or misdetection. The design of a recursive AOA tracker addressing these effects will increase the computational complexity and is outside the scope of the current paper.

The main objective of target tracking is to estimate the target state by using the 3D angle measurements collected by the moving own-ship. As the own-ship trajectory affects the final estimate performance significantly, it is important to determine the optimal path for the own-ship.

3. 3D PSEUDOLINEAR KALMAN FILTER

The relationship between angle measurements and target states is nonlinear [see (1)]. Pseudolinear Kalman filter (PLKF) [9] has many advantages in nonlinear target tracking compared with other recursive estimators [8, 9]. A 3D PLKF is developed which has a similar structure to the 3D PLE in [6].

3.1. The xy pseudolinear Kalman Filter

We define the target state vector in the 2D-projection xy-plane as $\boldsymbol{a}_k = [p_{xk}, \dot{p}_{xk}, p_{yk}, \dot{p}_{yk}]^T$. The target motion equation can be written as

$$\boldsymbol{a}_{k+1} = \boldsymbol{U}_k \boldsymbol{a}_k + \boldsymbol{u}_k \tag{3}$$

where $\boldsymbol{u}_k$ is the noise error in the state process [1], T denotes the constant time interval between discrete-time instants and

$$\boldsymbol{U}_k = \begin{bmatrix} \boldsymbol{A}_k & \boldsymbol{0}_{2\times2} \\ \boldsymbol{0}_{2\times2} & \boldsymbol{A}_k \end{bmatrix}, \quad \boldsymbol{A}_k = \begin{bmatrix} 1 & T \\ 0 & 1 \end{bmatrix}. \tag{4}$$

Rewriting (1a) similar to [16], the pseudolinear measurement model is

$$0 = [-\sin\tilde{\theta}_k, \cos\tilde{\theta}_k]\left([p_{xk}, p_{yk}]^T - [r_{xk}, r_{yk}]^T\right) + d_{xyk}\sin n_k \tag{5}$$

where $d_{xyk} = ||[p_{xk}, p_{yk}]^T - [r_{xk}, r_{yk}]^T||$. As $n_k \sim \mathcal{N}(0, \sigma_\theta^2)$, the pseudolinear noise satisfies $d_{xyk}\sin n_k \sim \mathcal{N}\left(0, d_{xyk}^2 \frac{1}{2}\left(1 - e^{-2\sigma_\theta^2}\right)\right)$ [9]. So the measurement noise variance is $e_k = d_{xyk}^2 \frac{1}{2}\left(1 - e^{-2\sigma_\theta^2}\right)$. In the filter calculation, the estimation information at time $k-1$ will be used to calculate the d_{xyk}.

Finally with the kth measurement, the xy pseudolinear Kalman filter takes the form [17, 18]

$$\boldsymbol{a}_{k|k-1} = \boldsymbol{U}_{k-1}\boldsymbol{a}_{k-1|k-1} \tag{6a}$$

$$\boldsymbol{W}_{k|k-1} = \boldsymbol{U}_{k-1}\boldsymbol{W}_{k-1|k-1}\boldsymbol{U}_{k-1}^T + \boldsymbol{M_{k-1}} \tag{6b}$$

$$\boldsymbol{h}_k = [-\sin\tilde{\theta}_k, 0, \cos\tilde{\theta}_k, 0] \tag{6c}$$

$$e_k = ||[\hat{p}_{xk|k-1}, \hat{p}_{yk|k-1}]^T - [r_{xk}, r_{yk}]^T||^2 \frac{1}{2}\left(1 - e^{-2\sigma_\theta^2}\right) \tag{6d}$$

$$\boldsymbol{k}_k = \boldsymbol{W}_{k|k-1}\boldsymbol{h}_k^T(\boldsymbol{h}_k\boldsymbol{W}_{k|k-1}\boldsymbol{h}_k^T + e_k)^{-1} \tag{6e}$$

$$y_k = \boldsymbol{h}_k\left(\boldsymbol{r}_{xyk} - \boldsymbol{a}_{k|k-1}\right) \tag{6f}$$

$$\boldsymbol{a}_{k|k} = \boldsymbol{a}_{k|k-1} + \boldsymbol{k}_k y_k \tag{6g}$$

$$\boldsymbol{W}_{k|k} = (\boldsymbol{I} - \boldsymbol{k}_k\boldsymbol{h}_k)\boldsymbol{W}_{k|k-1} \tag{6h}$$

where $\boldsymbol{W}_{k|k-1}$ denotes the covariance matrix and $\boldsymbol{M}_{k-1}$ is the model uncertainty covariance matrix [1] that satisfies

$$\boldsymbol{M}_{k-1} = \begin{bmatrix} q^x\boldsymbol{B}_{k-1} & \boldsymbol{0}_{2\times2} \\ \boldsymbol{0}_{2\times2} & q^y\boldsymbol{B}_{k-1} \end{bmatrix}, \quad \text{and} \quad \boldsymbol{B}_{k-1} = \begin{bmatrix} \frac{T^4}{4} & \frac{T^3}{2} \\ \frac{T^3}{2} & T^2 \end{bmatrix}. \tag{7}$$

3.2. The z pseudolinear Kalman Filter

Similarly, we define the target z-axis state vector as $\boldsymbol{b}_k = [p_{zk}, \dot{p}_{zk}]^T$ and the target dynamic model satisfies

$$\boldsymbol{b}_{k+1} = \boldsymbol{G}_k\boldsymbol{b}_k + \boldsymbol{w}_k \tag{8}$$

where $\boldsymbol{w}_k$ is the noise error in the state process and

$$\boldsymbol{G}_k = \begin{bmatrix} 1 & T \\ 0 & 1 \end{bmatrix}. \tag{9}$$

Equation (1b) can be rewritten as

$$d_{xyk}\tan\tilde{\phi}_k + [1,0][r_{zk}, \dot{r}_{zk}]^T = [1,0]\boldsymbol{b}_k + \frac{d_k}{\cos\tilde{\phi}_k}\sin m_k \tag{10}$$

where $m_k \sim \mathcal{N}(0, \sigma_\phi^2)$. The pseudolinear noise is $\frac{d_k}{\cos\tilde{\phi}_k}\sin m_k \sim \mathcal{N}\left(0, \frac{d_k^2}{\cos^2\tilde{\phi}_k}\frac{1}{2}\left(1 - e^{-2\sigma_\phi^2}\right)\right)$ (assume the noise is small) [6]. In the filter calculation, the estimation $[\hat{p}_{xk|k}, \hat{p}_{yk|k}]$ from the xy-PLKF will be used in the z-PLKF to calculate the d_{xyk} and d_k. Finally, the z pseudolinear Kalman filter takes the form

$$\boldsymbol{b}_{k|k-1} = \boldsymbol{G}_{k-1}\boldsymbol{b}_{k-1|k-1} \tag{11a}$$

$$\boldsymbol{S}_{k|k-1} = \boldsymbol{G}_{k-1}\boldsymbol{S}_{k-1|k-1}\boldsymbol{G}_{k-1}^T + \boldsymbol{N}_{k-1} \tag{11b}$$

$$\boldsymbol{l}_k = [1, 0] \tag{11c}$$

$$\hat{d}_{xyk} = ||[\hat{p}_{xk|k}, \hat{p}_{yk|k}]^T - [r_{xk}, r_{yk}]^T|| \tag{11d}$$

$$f_k = \frac{||[\hat{p}_{xk|k}, \hat{p}_{yk|k}, \hat{p}_{zk|k-1}]^T - [r_{xk}, r_{yk}, r_{zk}]^T||^2}{2\cos^2\tilde{\phi}_k}\left(1 - e^{-2\sigma_\phi^2}\right) \tag{11e}$$

$$\boldsymbol{t}_k = \boldsymbol{S}_{k|k-1}\boldsymbol{l}_k^T(\boldsymbol{l}_k\boldsymbol{S}_{k|k-1}\boldsymbol{l}_k^T + f_k)^{-1} \tag{11f}$$

$$c_k = \hat{d}_{xyk}\tan\tilde{\phi}_k + \boldsymbol{l}_k\left([r_{zk}, \dot{r}_{zk}]^T - \boldsymbol{b}_{k|k-1}\right) \tag{11g}$$

$$\boldsymbol{b}_{k|k} = \boldsymbol{b}_{k|k-1} + \boldsymbol{t}_k c_k \tag{11h}$$

$$\boldsymbol{S}_{k|k} = (\boldsymbol{I} - \boldsymbol{t}_k\boldsymbol{l}_k)\boldsymbol{S}_{k|k-1} \tag{11i}$$

where $\boldsymbol{N}_{k-1}$ is the dynamic model uncertainty covariance [1] that satisfies

$$\boldsymbol{N}_{k-1} = q^z\begin{bmatrix} \frac{T^4}{4} & \frac{T^3}{2} \\ \frac{T^3}{2} & T^2 \end{bmatrix}. \tag{12}$$

Combining the xy-PLKF and z-PLKF, the target state is $[\boldsymbol{a}_{k|k}; \boldsymbol{b}_{k|k}]_{6\times 1}$ and the final covariance matrix becomes

$$\left[\begin{array}{cc} \boldsymbol{W}_{k|k} & \mathbf{0}_{4\times 2} \\ \mathbf{0}_{2\times 4} & \boldsymbol{S}_{k|k} \end{array}\right]_{6\times 6}. \tag{13}$$

3.3. The condition for unbiased z-PLKF

Based on the z-PLKF equations in (10), we define the z-axis pseudolinear measurement as

$$z_k^{'} = \boldsymbol{l}_k \boldsymbol{b}_k + w_k^{'} \tag{14}$$

where $w_k^{'} = \frac{d_k}{\cos\tilde{\phi}_k} \sin m_k$ is the pseudolinear noise. As $\boldsymbol{l}_k = [1, 0]$ is a constant vector, the z-PLKF can be an unbiased estimator theoretically [6].

However, the ideal measurement $d_{xyk}\tan\tilde{\phi}_k + \boldsymbol{l}_k[r_{zk}, \dot{r}_{zk}]^T$ in (10) is not available in practical applications because the true distance d_{xyk} is unknown. Therefore, we can only use the biased estimate $\hat{d}_{xyk}$ from the xy-PLKF. Thus, the pseudolinear measurement contains a bias ζ_k determined by the xy-PLKF which is a variable with unknown distribution. Assume $\hat{d}_{xyk} = d_{xyk} + \zeta_k$, (14) becomes

$$\begin{aligned} z_k^{'} =& \boldsymbol{l}_k[r_{zk}, \dot{r}_{zk}]^T + d_{xyk}\tan\tilde{\phi}_k + \zeta_k \tan\tilde{\phi}_k \\ =& \boldsymbol{l}_k \boldsymbol{b}_k + w_k^{'} + \zeta_k \tan\tilde{\phi}_k. \end{aligned} \tag{15}$$

The final estimate of z-axis will be biased because ζ_k is unknown.

From equation (15) we find that when $\tilde{\phi}_k$ equals zero, the bias from xy-PLKF will be eliminated perfectly.

Lemma: When the elevation angle measurement equals zero, the z-PLKF will be unbiased.

Proof. When $\tilde{\phi}_k = 0$, the z-PLKF equations in (11) become

$$\boldsymbol{b}_{k|k-1} = \boldsymbol{G}_{k-1}\boldsymbol{b}_{k-1|k-1} \tag{16a}$$

$$\boldsymbol{S}_{k|k-1} = \boldsymbol{G}_{k-1}\boldsymbol{S}_{k-1|k-1}\boldsymbol{G}_{k-1}^T + \boldsymbol{N}_{k-1} \tag{16b}$$

$$\boldsymbol{l}_k = [1, 0] \tag{16c}$$

$$f_k = \frac{||[\hat{p}_{xk|k}, \hat{p}_{yk|k}, \hat{p}_{zk|k-1}]^T - [r_{xk}, r_{yk}, r_{zk}]^T||^2}{2}\left(1 - e^{-2\sigma_\phi^2}\right) \tag{16d}$$

$$\boldsymbol{t}_k = \boldsymbol{S}_{k|k-1}\boldsymbol{l}_k^T(\boldsymbol{l}_k\boldsymbol{S}_{k|k-1}\boldsymbol{l}_k^T + f_k)^{-1} \tag{16e}$$

$$c_k = \boldsymbol{l}_k\left([r_{zk}, \dot{r}_{zk}]^T - \boldsymbol{b}_{k|k-1}\right) \tag{16f}$$

$$\boldsymbol{b}_{k|k} = \boldsymbol{b}_{k|k-1} + \boldsymbol{t}_k c_k \tag{16g}$$

$$\boldsymbol{S}_{k|k} = (\boldsymbol{I} - \boldsymbol{t}_k\boldsymbol{l}_k)\boldsymbol{S}_{k|k-1}. \tag{16h}$$

The new z-PLKF becomes an ordinary linear Kalman filter with constant observation matrix $\boldsymbol{l}_k = [1, 0]$ [17]. Because the ordinary Kalman filter is unbiased, the z-PLKF also becomes unbiased. □

4. PATH OPTIMIZATION STRATEGIES FOR THE 3D-PLKF

4.1. Gradient-descent algorithm for the xy-PLKF

In order to improve tracking performance, gradient-descent path optimization [11] is applied with the xy-PLKF. Mean squared error (MSE) is used to evaluate the estimation performance.

We define the cost function based on the xy-PLKF as

$$J(\boldsymbol{r}_{xyk}) = \left[\begin{array}{c} J(r_{xk}) = \text{tr}(\boldsymbol{W}_{k|k}) \\ J(r_{yk}) = \text{tr}(\boldsymbol{W}_{k|k}) \end{array}\right] \tag{17}$$

where tr$(\boldsymbol{W}_{k|k})$ is the trace of the xy-PLKF covariance matrix and $\boldsymbol{r}_{xyk} = [r_{xk}, r_{yk}]^T$ is the own-ship location in xy-plane at time k. In the optimization, the next waypoint $\boldsymbol{r}_{xyk+1}$ of the own-ship needs to satisfy the relationship below [11]

$$\boldsymbol{r}_{xyk+1} = \boldsymbol{r}_{xyk} - v_{xy}T\frac{\frac{\partial J(\boldsymbol{r}_{xyk})}{\partial \boldsymbol{r}_{xyk}}}{\left\|\frac{\partial J(\boldsymbol{r}_{xyk})}{\partial \boldsymbol{r}_{xyk}}\right\|} \tag{18}$$

where v_{xy} is the sensor velocity in xy-plane. The objective of minimizing $J(\boldsymbol{r}_{xyk})$ becomes finding the largest gradient $\frac{\partial J(\boldsymbol{r}_{xyk})}{\partial \boldsymbol{r}_{xyk}}$. From (18), the local gradient vector at the own-ship kth position can be calculated by

$$\frac{\partial J(\boldsymbol{r}_{xyk})}{\partial \boldsymbol{r}_{xyk}} = \left[\begin{array}{c} \frac{\partial J(r_{xk})}{\partial r_{xk}} \approx \frac{J(r_{xk}+\delta) - J(r_{xk})}{\delta} \\ \frac{\partial J(r_{yk})}{\partial r_{yk}} \approx \frac{J(r_{yk}+\delta) - J(r_{yk})}{\delta} \end{array}\right] \tag{19}$$

where δ is a next step distance. To obtain $J(r_{xk}+\delta)$ and $J(r_{yk}+\delta)$, we also need to calculate the probable next step pseudolinear measurement matrix $\boldsymbol{h}_{k+1}$. Besides, the probable next step pseudolinear noise variance e_{k+1} which is required in $\boldsymbol{h}_{k+1}$ calculation can be rebuilt by substituting $r_{xk} + \delta$ and $r_{yk} + \delta$ into (6d), respectively. Then based on (6), $\boldsymbol{W}_{xk+1|k}$ and $\boldsymbol{W}_{yk+1|k}$ are obtained and we get

$$\begin{aligned} J(r_{xk} + \delta) &= \text{tr}(\boldsymbol{W}_{xk+1|k}) \\ J(r_{yk} + \delta) &= \text{tr}(\boldsymbol{W}_{yk+1|k}). \end{aligned} \tag{20}$$

Substituting (19) and (20) into (18), the own-ship next waypoint is obtained by

$$\boldsymbol{r}_{xyk+1} = \left[r_{xk} - \frac{v_{xy}T\frac{\partial J(r_{xk})}{\partial r_{xk}}}{||\frac{\partial J(\boldsymbol{r}_{xyk})}{\partial \boldsymbol{r}_{xyk}}||}, \quad r_{yk} - \frac{v_{xy}T\frac{\partial J(r_{yk})}{\partial r_{yk}}}{||\frac{\partial J(\boldsymbol{r}_{xyk})}{\partial \boldsymbol{r}_{xyk}}||} \right]^T. \tag{21}$$

In the gradient calculation, the noise variance e_k, next step pseudolinear measurement vector $\boldsymbol{h}_{k+1}$ and gain matrix $\boldsymbol{k}_{k+1}$ are required that can be re-calculated based on (6).

4.2. Grid search path optimization for the z-PLKF

As it is impossible to calculate the gradient-descent vector in z-axis only, grid search method is used. To minimize the estimation MSE, the cost function is defined as

$$J(r_{zk}) = \text{tr}(\boldsymbol{S}_{k|k}). \tag{22}$$

The possible next waypoints are represented as

$$\boldsymbol{\Phi}(r_{zk+1}) = \left[r_{zk}, ..., r_{zk} \pm (N-1)\frac{v_{xyz}T}{N}, r_{zk} \pm N\frac{v_{xyz}T}{N}\right]^T \tag{23}$$

where $\boldsymbol{\Phi}(r_{zk+1})$ is the possible next waypoint vector, N is the grid search radius that determines how many points will be calculated, v_{xyz} is own-ship velocity. Note that $v_z = \frac{r_{zk+1} - r_{zk}}{T}$ and $v_{xyz}^2 = v_{xy}^2 + v_z^2$. The cost function values of possible next waypoints are acquired by substituting each elements of $\boldsymbol{\Phi}(r_{zk+1})$ into (11). The optimal next waypoint is obtained from

$$r_{zk+1} = \underset{\boldsymbol{\Phi}(r_{zk+1})}{\text{argmin}}\ J(r_{zk+1}). \tag{24}$$

The final 3D path optimization algorithm is from (21) and (24) and they are decoupled.

5. SIMULATION STUDIES

In the simulation examples, the target is at $[1000, 1000, 1000]m$ originally with the velocities $[5, 5\sin(\frac{k\pi}{150}), 1]m/s$. Besides, the target acceleration error variances are $[0.5^2, 0.5^2, 0.1^2]m^4/s^4$. The own-ships move from different places. Own-ship 1, 2 and 3 start from $[0, 0, 0]m$, $[2000, 2000, 300]m$ and $[-100, 1800, 2000]m$, separately. The own-ships have a same velocity $v_{xyz} = 70m/s$. The time interval is $T = 1s$ with 300 measurement points and $\delta = 70m$. The sensor measurement noises are $\sigma_\theta = \sigma_\phi = 1^o$. The estimator initial parameters are $\boldsymbol{a}_{0|0} = [1400, 9, 800, 13]^T$, $\boldsymbol{b}_{0|0} = [1100, 5]^T$, $\boldsymbol{W}_{0|0} = \text{diag}[10^4, 10^4, 10^4, 10^4]$ and $\boldsymbol{S}_{0|0} = \text{diag}[10^4, 10^4]$. 21 points are picked in the grid search optimization. The filters assume $q^x = q^y = q^z = 10^{-2}$. A no fly sphere around the target with $500m$ radius is maintained. The algorithm of how to avoid the no fly area is similar to [11]. Own-ship 4 starts from $[0, 0, 0]m$ and uses an 3D EKF gradient-descent path optimization method as a comparison. The EKF initial parameters are $[\boldsymbol{a}_{0|0}; \boldsymbol{b}_{0|0}]$ and $\text{diag}[\boldsymbol{W}_{0|0}, \boldsymbol{S}_{0|0}]$. The whole estimate and path optimization process is repeated with 500 Monte Carlo runs. The bias and root-mean-squared-errors (RMSE) are calculated by using 500 Monte Carlo runs. Collision problem is ignored.

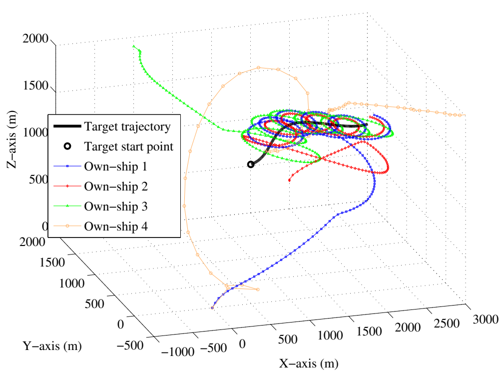

Fig. 2. Trajectories of the target and own-ship.

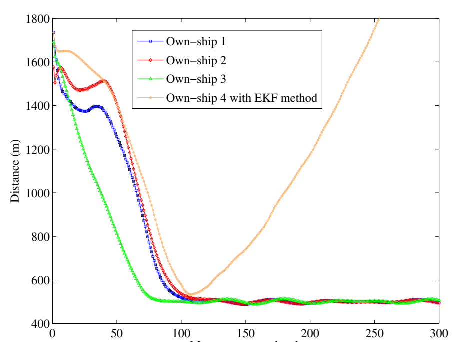

Fig. 3. Evolutions of the distance between own-ships and target.

Table 1. Elevations of the target and own-ships

elevation \ k	25	50	100	150	200	300
Target (m)	1025	1050	1100	1150	1200	1300
Own-ship 1(m)	840	1028	1099	1149	1199	1299
Own-ship 2(m)	1029	1068	1098	1149	1199	1299
Own-ship 3(m)	1252	1049	1099	1149	1199	1298
Own-ship 4(m)	439	1537	1371	1208	1257	1331

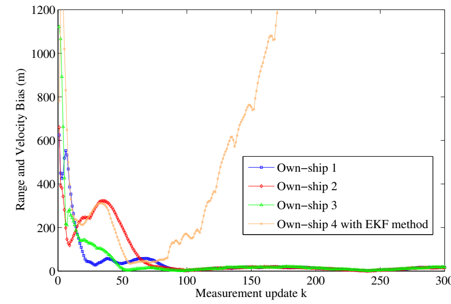

Fig. 4. Evolutions of the range and velocity bias.

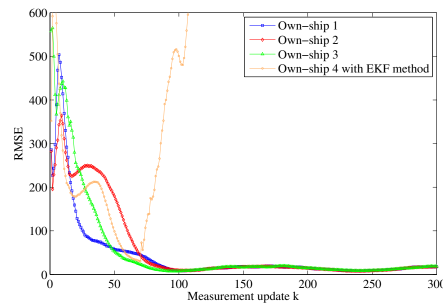

Fig. 5. Evolutions of the RMSE.

Fig. 2 shows the mean trajectories of the target and own-ships. Fig. 3 shows the mean distance changes between own-ships and the true target. The own-ships using PLKF method reach the no fly area and follow the target with spiral paths. While the trajectory of own-ship 4 shows a tendency of flying away from the target. The elevations of the own-ships and target are shown in Table 1. The results from Table 1 match the lemma in Section 3.3.

Fig. 4 and Fig. 5 provide the mean bias and RMSE performance of the different own-ships. The bias cannot be eliminated because of the process noise (modeling and acceleration error). From Fig. 4 and Fig. 5, the bias and RMSE of the three PLKF examples all show a tendency of converging to a small value. In Fig. 4, at the early period of tracking process, bias increases because the cost function is the trace of the covariance matrix rather than the bias. Besides, the estimation performance is impacted by the start points significantly. The performance of own-ship 1 is also better than the performance of own-ship 4 before the divergence problem. This divergence problem may happen when the state model becomes very different from the real target. The acceleration noise also makes the EKF unstable.

6. CONCLUSION

In this paper we have proposed a 3D PLKF and an own-ship path optimization algorithm for 3D AOA target tracking. First, the nonlinear azimuth and elevation angle measurements were transformed into pseudolinear models. Next, a 3D PLKF was developed consisting of an xy-PLKF and a z-PLKF. We showed that when the own-ship and target are at the same height, the z-PLKF becomes unbiased. The gradient-descent method was applied in the xy-plane path optimization by minimizing the MSE. As the gradient-descent vector is impossible to obtain for the z-axis, a grid search optimization method was designed for the z-axis path optimization. Simulation examples verified the effectiveness of the proposed algorithm. The future work will consider using multiple own-ships to track multiple targets with distributed estimation and path optimization strategies.

7. REFERENCES

[1] Y. Bar-Shalom, “Multitarget-multisensor tracking: Applications and advances. volume iii,” *Norwood, MA, Artech House, Inc., 2000*, 2000.

[2] K. Doğançay, “UAV path planning for passive emitter localization,” *Aerospace and Electronic Systems, IEEE Transactions on*, vol. 48, no. 2, pp. 1150–1166, 2012.

[3] J.A. Fawcett, “Effect of course maneuvers on bearings-only range estimation,” *Acoustics, Speech and Signal Processing, IEEE Transactions on*, vol. 36, no. 8, pp. 1193–1199, 1988.

[4] L. Badriasl and K. Dogancay, “Three-dimensional target motion analysis using azimuth/elevation angles,” *Aerospace and Electronic Systems, IEEE Transactions on*, vol. 50, no. 4, pp. 3178–3194, 2014.

[5] K. Doğançay, “Bias compensation for the bearings-only pseudolinear target track estimator,” *Signal Processing, IEEE Transactions on*, vol. 54, no. 1, pp. 59–68, Jan 2006.

[6] K. Dogancay, “3D pseudolinear target motion analysis from angle measurements,” *Signal Processing, IEEE Transactions on*, vol. 63, no. 6, pp. 1570–1580, March 2015.

[7] K. Doğançay and Ibal G., “Instrumental variable estimator for 3D bearings-only emitter localization,” in *Intelligent Sensors, Sensor Networks and Information Processing Conference, 2005. Proceedings of the 2005 International Conference on*, Dec. 2005, pp. 63–68.

[8] V.J. Aidala, “Kalman filter behavior in bearings-only tracking applications,” *Aerospace and Electronic Systems, IEEE Transactions on*, , no. 1, pp. 29–39, 1979.

[9] V.J. Aidala and S.C. Nardone, “Biased estimation properties of the pseudolinear tracking filter,” *Aerospace and Electronic Systems, IEEE Transactions on*, , no. 4, pp. 432–441, 1982.

[10] T.L. Song and J.L. Speyer, “A stochastic analysis of a modified gain extended kalman filter with applications to estimation with bearings only measurements,” *Automatic Control, IEEE Transactions on*, vol. 30, no. 10, pp. 940–949, 1985.

[11] K. Doğançay, “Single-and multi-platform constrained sensor path optimization for angle-of-arrival target tracking,” in *18th European Signal Processing Conference (EUSIPCO-2010), Aalborg, Denmark*, 2010, pp. 835–839.

[12] Y. Oshman and P. Davidson, “Optimization of observer trajectories for bearings-only target localization,” *Aerospace and Electronic Systems, IEEE Transactions on*, vol. 35, no. 3, pp. 892–902, 1999.

[13] K. Doğançay and H. Hmam, “Optimal angular sensor separation for AOA localization,” *Signal Processing*, vol. 88, no. 5, pp. 1248–1260, 2008.

[14] S.Y. Zhao, B.M. Chen, and T.H. Lee, “Optimal sensor placement for target localization and tracking in 2D and 3D,” *International Journal of Control*, vol. 86, no. 10, pp. 1687–1704, 2013.

[15] S. Xu and K. Doğançay, “Optimal sensor deployment for 3D AOA target localization,” in *Acoustics, Speech and Signal Processing (ICASSP), 2015 IEEE International Conference on*. IEEE, 2015, pp. 2544–2548.

[16] S.C. Nardone, A.G. Lindgren, and K.F. Gong, “Fundamental properties and performance of conventional bearings-only target motion analysis,” *Automatic Control, IEEE Transactions on*, vol. 29, no. 9, pp. 775–787, 1984.

[17] D. Simon, *Optimal state estimation: Kalman, H infinity, and nonlinear approaches*, John Wiley & Sons, 2006.

[18] M.S. Grewal and A.P. Andrews, *Kalman filtering: theory and practice using MATLAB*, John Wiley & Sons, 2011.